# Mid-Infrared Laser Spectroscopy Applications I: Detection of Traces of High Explosives on Reflective and Matte Substrates

*Leonardo C. Pacheco-Londoño, John R. Castro-Suarez,*
*Nataly J. Galán-Freyle, Amanda M. Figueroa-Navedo,*
*José L. Ruiz-Caballero, Ricardo Infante-Castillo*
*and Samuel P. Hernández-Rivera*

## Abstract

Mid-infrared (MIR) lasers have revolutionized infrared vibrational spectroscopy, converting an already dominant spectroscopic analysis technique into an even more powerful, easier to use, and quicker turn-around cadre of versatile spectroscopic tools. A selection of applications, revisited under the umbrella of MIR laser-based properties, very high brightness, collimated beams, polarized sources, highly monochromatic tunable sources, and coherent sources, is included. Applications discussed concern enhanced detection, discrimination, and quantification of high explosives (HEs). From reflectance measurements of chemical residues on highly reflective metallic substrates to reflectance measurements of HEs deposited on non-reflective, matte substrates is discussed. Coupling with multivariate analyses (MVA) techniques of Chemometrics allowed near trace detection of HEs, with sharp discrimination from highly MIR absorbing substrates.

**Keywords:** mid-infrared (MIR) laser spectroscopy, quantum cascade lasers (QCLs), high explosives (HEs), multivariate analyses (MVA), Chemometrics

## 1. Introduction

Vibrational spectroscopy, in its two main branches: infrared spectroscopy (IRS) and Raman scattering (RS) are used for identifying and quantifying samples in complex matrices because each substance has a unique spectrum in the fingerprint and fundamental vibrations regions of the electromagnetic spectrum and the corresponding Raman shift regions [1–6]. IRS is a well-established discipline within science and technology fields, and it has continuously evolved over the past 200 years [1–3]. Throughout this time, IRS gradually developed all its major modalities: absorption/transmission, reflection, and emission spectroscopies. It has benefited from technological developments in spectral sorting capabilities (gratings instead of prisms; interferometers instead of dispersive spectrometers), improvements in

detection technologies, development of water-resistant optical elements, and in fast processing data analysis: Fourier transformation [1–6]. However, one area that has lagged developments and improvements until very recently has been in excitation sources of infrared spectra. Only thermal sources (globars), which are inherently low power sources been traditionally available for bench and portable systems [3].

Both IRS and RS, in their various modalities, have been shown useful for characterization, detection, identification, and quantification of threat chemicals, among them high explosives (HEs) and homemade explosives (HMEs) [6–18]. In the past 25 years, the techniques have frequently been used in a remote mode to fight terrorist threats establishing the base for the essential countermeasures to inhibit explosives events. Research in areas of interest to security and national defense with a focus on detection of HEs has been reviewed [7–18].

The difference in inherent strength of the photonic mechanisms that enable IRS and RS as the dominant techniques of vibrational molecular spectroscopy limits their capabilities and use in applications of remote detection of threat chemical compounds. IRS being a photonic absorption process is a much stronger mechanism than the inelastic scattering of photons in a Raman event. This fact enables remote infrared spectroscopy (RIRS) with the capability of near trace detection of target chemicals up to tens of meters. On the other hand, RS is supported by important properties of laser technology, which enable remote sensing at distances as long as 1 km, but it is limited to the detection of bulk or semi-bulk amounts of samples (as low as several μg) and small gaseous molecules, due to the weakness of the scattering event [19–26].

The need for developing more powerful mid-infrared (MIR) sources that would allow detection at longer ranges when a target hazardous threat chemical is located on a solid substrate in the form of a residue at trace or near trace level amounts requires the use lasers sources for the task. MIR laser sources were introduced in with the invention of the quantum cascade laser (QCL) [27]. QCLs slowly developed from narrow band operation to widely tunable, multi-diode systems initially producing a few milli Watts of power to current commercial systems, capable of delivering high powers and enabling detection of hazardous chemical compounds remotely [28–34].

QCLs can be used to detect gases and vapors and even high sublimation pressure chemicals, such as triacetone triperoxide (TATP) a cyclic organic peroxide HME. Pentaerythritol tetranitrate (PETN) an aliphatic nitrate ester, 1,3,5-trinitroperhydro-1,3,5-triazine (RDX) an aliphatic nitramine, and 2,4-dinitrotoluene (2,4-DNT) and 2,4,6-trinitrotoluene (TNT) nitroaromatic HEs, have very low sublimation pressures and have been detected as particle residues on substrates using photoacoustic spectroscopy [35–37]. Vapor phase detection of TATP and TNT has also been attained using IRS with adequate results [37, 38]. QCL sources have also been used for remote detection of HEs deposited on solid substrates using reflectance, photoacoustic, and hyperspectral imaging [39–44].

However, previous research in this field has generally centered on the detection of HEs deposited reflective substrates [42]. Only one report addressed the problem of detection of HEs on matte surfaces [44]. The work of Pacific Northwest National Lab researchers in the spectroscopic and angular dependence of MIR diffuse scattering from explosives residues deposited on a painted car door using an external cavity QCL (EC-QCL) was measured laid the foundation for detection of HE on matte surfaces [43]. Intensity dependence on the angle of the source-target-detector in active mode RIRS [45], the dependence of the limit of detection (LOD) on angular position, surface type, and analyte concentration for active mode RIRS using globars, modulated and non-modulated, have also been measured [46].

## 2. General specifications of scanning QCL spectrometers

The necessity of collimated and coherent light sources in the MIR region is evident by the limitation in the operational distance of RIRS experiments based on thermal sources. Even when coupled to IR telescopes to direct the light source of the substrates containing the target HEs, the energy/area of these systems can greatly benefit from a monochromatic, coherent, collimated and polarized source: a laser. The development of lasers with the ability to emit radiation in the 3–12 μm (833–3330 cm$^{-1}$) spectroscopic range has advanced dramatically with the development lasers [27, 47, 48]. MIR laser spectroscopy offers the possibility to detect threat chemicals, both in the vapor phase (high sublimation pressure HEs, such as TATP) as well as traces deposited on substrates. A remote detection scheme for low vapor pressure nitroexplosives was described by Bauer et al. [36] QCLs are highly suitable for compact and rugged sensor devices used for security and defense applications.

Block Engineering (BE; Southborough, MA, USA) developed a scanning QCL pre-dispersive spectrometer (LaserScan™) operating in the 6–12 μm (830–1670 cm$^{-1}$) spectral range. This QCL spectrometer offers some key advantages over other established technologies in developing the applications discussed in this contribution, namely:

1. Speed: very fast scanning and inspection of surfaces due to the use of a large 2–4-mm beam spot, long remote distance and high pulse rate lasers.

2. Ease of use: the system uses a collimated beam with fixed optics that allows operating at a convenient, safe remote minimum distance of 1–2 m.

3. Detection of multiple threat chemicals: including HEs, HMEs, mixes, formulations, and essentially any substance that has a spectral feature in the range 6–12 μm.

4. Detection of all states of substances: liquids, gases, and vapors, in addition to its current capacity of surface detection.

5. Personnel safety: non-focusing laser beam operating in the 6–12 μm spectral region avoids eye safety issues.

6. High sensitivity measurements: high-power laser source enables detection of low chemical concentrations on surfaces: 1–15 μg/cm$^2$ (0.01–0.15 g/m$^2$) and bulk materials.

This LaserScan™ spectroscopic system was designed for detection of surface contaminants. The system can acquire reflectance spectra of films and deposits of chemicals on reflective substrates. The initial stage of development of applications of MIR lasers involved validation experiments aimed at evaluating the performance of the QCL LaserScan™ in the goal of detecting HEs on metal surfaces. Some of the results obtained with the QCL LaserScan™ system and corresponding FTIR reference (Ref) spectra are shown in **Figure 1**.

There are operational parameters worth discussing in some detail. Two aligning He:Ne lasers can be turned on to focus the invisible MIR laser beam of the spectrometer. The unit was designed for short focal length work, and the two He:Ne beams converge at the focal length of 15 ± 3 cm. Since these units were designed to operate in reflectance mode, smooth reflective metal substrates, such as Al, stainless
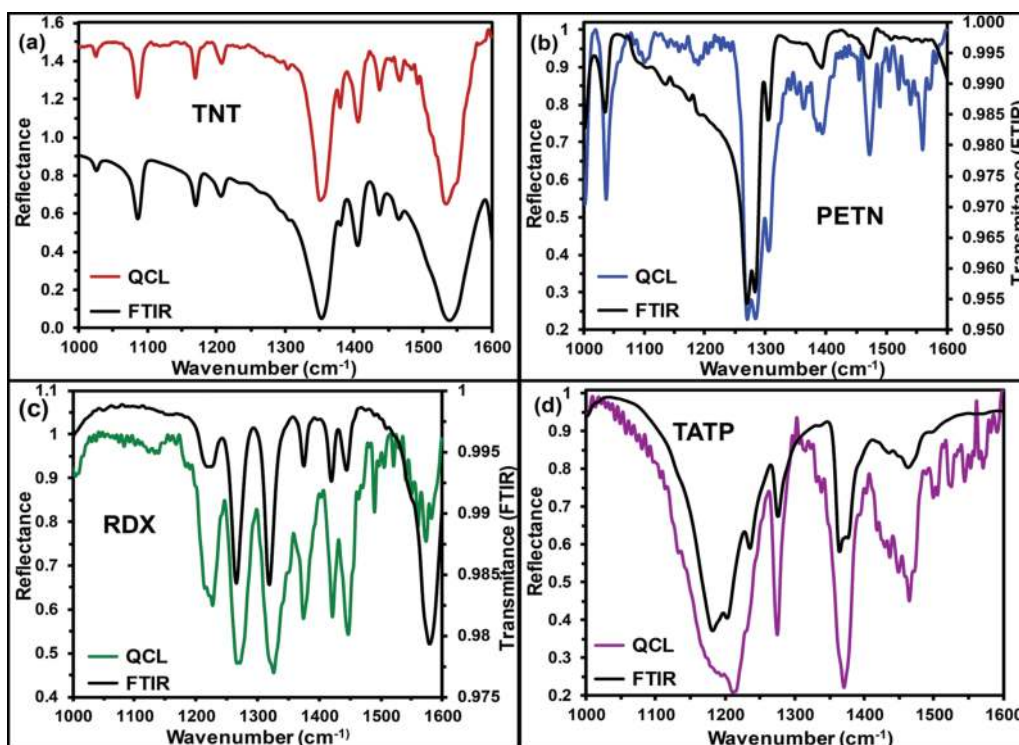
**Figure 1.**
*QCL and FTIR (reference) spectra of HEs on reflective Al plates: (a) TNT, (b) PETN, (c) RDX and (d) TATP.*

steel (SS), gold, etc., were used for the initial experiments. However, defocusing the MIR laser beam was required when measuring the spectra of chemicals deposited on highly reflective metallic surfaces since the specular radiation collected in back reflection mode saturated the detector. Alternatively, tilting the metallic substrate to 9–10° avoided detector saturation. The reflectance spectra measured with QCL and FTIR (reference) of (a) TNT, (b) PETN, (c) RDX and (d) TATP are shown in **Figure 1**. The MIR laser spectra were collected on a smooth aluminum (Al) substrate. These spectra, as well as other acquired, serve the purpose of validating the proposed technique for detection of neat HEs, mixtures, and formulations, and HME and their chemical precursors. The MIR laser spectra were acquired at open-air conditions. Thus, water vapor lines can be observed for some of the spectra, particularly for TATP samples, which are rapidly sublimating even at room temperature. In other cases, the inherent strength of the MIR signatures of the HEs makes the water vapor lines imperceptible.

## 3. MIR laser spectroscopy detection of HE on matte substrates

A MIR laser spectrometer was used to acquire reflectance spectra of HEs coatings on matte, low reflectivity substrates such as travel bags (TB; polyester), cardboard (CB), and wood (W). Various deposition methods including smearing, partial immersion, spin coating, and air spray were used for transferring the HEs to the substrates used in the study. The HEs used included nitroaromatic explosive (TNT), aliphatic nitrate ester (PETN), and aliphatic nitramine (RDX). Multivariate analysis (MVA) algorithms were used to analyze the data. Partial least squares (PLS) regression analysis was applied to correlate the intensity of the reflectance bands to the surface loadings of the HE deposited on the substrates. Moreover,

discriminant analysis (DA) combined with PLS (PLS-DA) to identify similarities of HEs and to discriminate spectral features of one type of HE from other types of HEs and substrates [49–51]. The data was pre-treated with Chemometrics algorithms to prepare the reflectance spectra of the explosives deposited on the matte surfaces studied. The results demonstrated that the MIR laser spectroscopy method presented can be used for detection and discrimination of HEs on non-reflective substrates when a supervised model has been previously constructed or when a reference spectrum of the neat substrate can be acquired to be subtracted from the HE/substrate spectrum. Low surface loadings (1–15 $\mu g/cm^2$) of HEs were used in the investigation.

## 3.1 Spectral analysis

Reflectance spectra of selected HEs deposited on matte substrates used for the investigation were acquired using the LaserScan™. The MIR region, where fundamental modes of vibration of HEs are located (1000–1600 $cm^{-1}$), such as the symmetric and asymmetric $NO_2$ modes, was scanned. Representative QCL reflectance spectra of HEs/substrates are illustrated in **Figure 2**. Spectra of HE/Al have been included as reference spectra to help in the assignment of the vibrational markers of the HEs on the non-reflective substrates. Distinctive vibrational signatures of TNT, PETN, and RDX are illustrated in **Figure 2a**. These spectra evidence the reflective nature of the metallic substrate. Tentative assignments for TNT include $CH_3$ deformation (1024 $cm^{-1}$), C–H ring in-plane bending (1086 $cm^{-1}$), nitro groups symmetric stretching (1350 $cm^{-1}$) and $NO_2$ asymmetric stretching (1551 $cm^{-1}$) [52]. PETN vibrational signatures included CO stretching (1003 $cm^{-1}$), $NO_2$ rocking (1038 $cm^{-1}$), $ONO_2$ rocking (1272 $cm^{-1}$), $NO_2$ stretching (1285 $cm^{-1}$) and $NO_2$
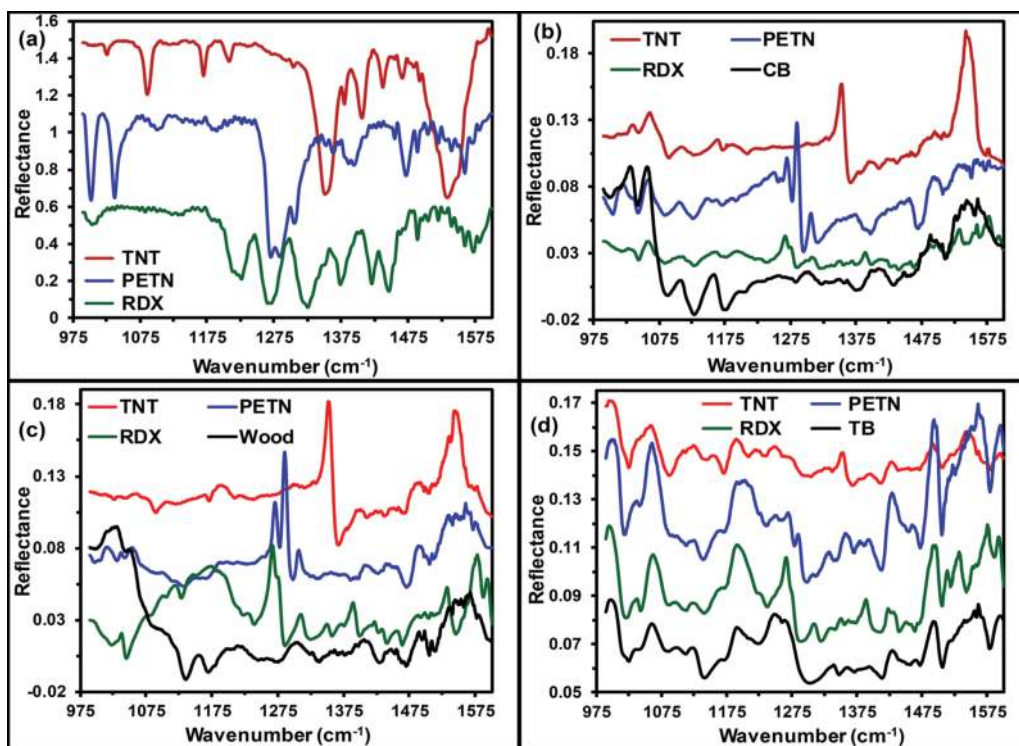


**Figure 2.**
*QCL spectra of HEs on substrates studied: (a) Al, reference reflective substrate; (b) CB; (c) wood (W); and (d) TB. Surface concentrations were kept constant at ~15 $\mu g/cm^2$ for comparison purposes. Reflectance spectra of matte substrates are included to denote the extent of spectroscopic intrusion.*

rocking (1306 cm$^{-1}$) [53, 54]. Vibrational markers for RDX included N–N and ring stretching (997 cm$^{-1}$), C–N stretching (1220 cm$^{-1}$), NO$_2$ stretching (1270 cm$^{-1}$), N–N stretching (1310 cm$^{-1}$), H–C–N asymmetric bending (1420 and 1445 cm$^{-1}$) and N–O asymmetric stretching (1570 cm$^{-1}$) [55, 56]. The HEs signatures detected agree well with literature values. The QCL spectroscopic features of the NO$_2$ group markers from the HEs deposited on the matte substrates used in the investigation differed slightly from those of HEs/Al. When the HEs were deposited on matte surfaces, the vibrational markers were inverted with respect to the corresponding markers of HEs deposited on reflective substrates. Suter et al. also described the same effect when studying the QCL reflectance spectra of TNT deposited on a painted car door [43].

The reflectance of a material is a measure of its capacity to reflect incident light. It is mainly based on: the portion of the incident radiation reflected from the material surface of and the incident power of the radiation at a given wavenumber interval. It is customary to represent reflectance spectra as the ratio of the reflected MIR light from the sample surfaces to the reflected MIR light from the reference surface (Al plate). This is called the relative reflectance. When the HEs were deposited on metallic substrates, such as Al, the intensity of the reflected light was lower in the spectral region where the HEs have MIR signals. This generated "downward" peaks because of the light power loss at the MIR active band location when calculating the relative reflectance spectrum (**Figure 2a**). For samples with HEs deposited on low matte surfaces (such as TB, CB, W) alterations in the optical characteristics of the surfaces took place such that the intensities of the light reflected from the HE/surface combinations was higher in the spectral locations in which the HEs have MIR peaks, generating inverted or "upward" signals.

## 3.2 Chemometrics analyses

Two MVA routines were used to analyze the laser reflectance spectra: principal component analysis (PCA) and partial least squares (PLS). PCA was employed to classify similarities in a spectral data set, and PLS was used to find the best correlation between the MIR signatures and the surface concentration of the HEs. MVA routines used were highly efficient in achieving the objectives of this research. MVA pre-treatment routines were applied to the QCL reflectance spectra of HEs/substrates combinations. Chemometrics routines used to enhance the detection of target HEs deposited on TB, and CB required only first derivative (1st dvt) and mean centering (MC) as preprocessing routines. W substrates were more challenging for generating efficient PCA models and required a third pre-treatment of the data: standard normal variate (SNV) transformation to achieve discrimination of the HEs from the substrates. Classification according to the type of HE was also attained. A general PCA model of TNT, PETN, and RDX on TB, CB, and W enabled the discrimination even in the presence of highly MIR absorbing and complex matrices. A total of 12 principal components (PCs) were required to capture a variance of 80%. Hence, MIR laser spectroscopy was shown useful in the detection of HEs on matte surfaces. When coupled with powerful Chemometrics routines, such as PCA, the technique was successful in discriminating the HEs from the highly interfering substrates investigated. Some of the results using PCA models were: **Figure 3a** shows PCA for HE/TB; **Figure 3b** shows the PCA regression model for TNT, PETN, RDX on TB, CB, W (grand model: all HEs/all substrates).

PLS models were highly efficient in predicting the surface loadings of the HEs on the matte surfaces with eight latent variables (LVs) obtaining values of the correlation coefficients (R$^2$) higher than 0.9. This validates that the developed
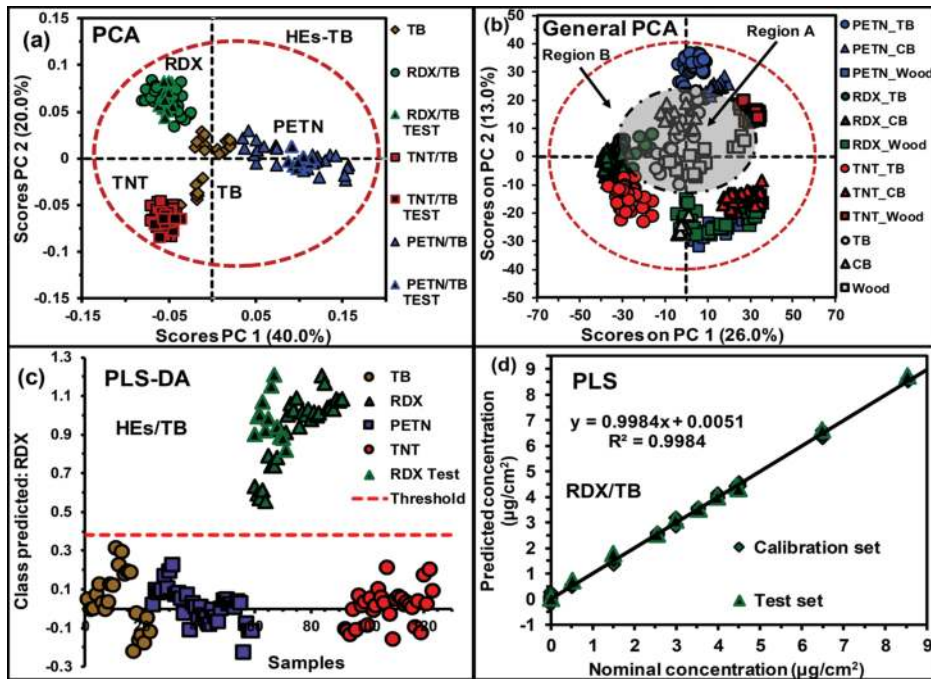
**Figure 3.**
*(a) PCA model for QCL detection of HE/TB; (b) general PCA regression model for QCL spectra of HE/substrates. The dotted red closed curve represents a 95% confidence level. (c) Class prediction of HE on TB using PLS-DA; (d) PLS predicted vs. nominal surface concentration of RDX/TB with a correlation coefficient ($R^2$) of 0.9984.*

methodology can be used for the detection of HEs on highly MIR absorbing matte substrates. **Figure 3c** shows an example the resulting from the discrimination of a matte substrate (TB) using the developed PLS-DA models. Discrimination of each HE from the others and the substrate are illustrated in the figure as an example. Four LVs were used to obtain the best MVA classification model with high sensitivity (see **Table 1**), for the data sets of calibration, cross-validation, and prediction. The total variance accounted for was 87.8%, which is sufficiently effective for a good classification of the predicted spectroscopic set on TB. For the Chemometrics cluster analysis of HEs/TB, six LVs were used to retain 80% of the variance of the spectral data. As shown in the score plot in **Figure 3d**, two LVs that captured 60% of

| Substrate | Explosive | LV | $R^2$ CV | $R^2$ Pred | RMSECV (µg/cm$^2$) | RMSEP (µg/cm$^2$) |
|-----------|-----------|----|----------|-----------|--------------------|--------------------|
| TB | PETN | 8 | 0.998 | 0.999 | 0.12 | 0.09 |
| | RDX | 8 | 0.996 | 0.998 | 0.17 | 0.13 |
| | TNT | 8 | 0.973 | 0.971 | 0.48 | 0.41 |
| CB | PETN | 7 | 0.980 | 0.985 | 0.56 | 0.41 |
| | RDX | 8 | 0.980 | 0.987 | 0.61 | 0.40 |
| | TNT | 8 | 0.945 | 0.993 | 1.06 | 0.47 |
| Wood | PETN | 5 | 0.989 | 0.996 | 0.43 | 0.29 |
| | RDX | 8 | 0.984 | 0.985 | 0.46 | 0.39 |
| | TNT | 9 | 0.918 | 0.982 | 1.03 | 0.45 |

**Table 1.**
*PLS parameters of calibrations for QCL spectra of HEs deposited on substrates.*

the variance was enough to attain a very good classification and to discriminate the HEs from the non-reflective surfaces. Spectra from the prediction sets: RDX-Test, TNT-Test, and PETN-Test were all well grouped according to chemical properties with spectra from the calibration sets.

**Figure 4** shows some of the HE/substrates surface concentration profiles generated and an illustration of how obtaining difference spectra can easily result in analytes identification. Similar spectra were used to prepare surface concentration profiles in preparation to perform quantitative Chemometrics runs. A sample set consisting of nine surface concentration profiles, three-HEs × three-substrates (plus three replicas of each combination), was assembled. Non dosed, clean Al substrates were used as background. **Figure 4a** shows some of the RDX spectra recorded on W substrates. **Figure 4b** shows spectra for TNT on CB at various surface concentrations. **Figure 4c** shows measured QCL reflectance spectra for PETN on wood. The QCL-based methodology proposed for detecting HEs on matte substrates does not necessitate the use of MVA for identifying the HEs. As shown in **Figure 4d**, a reflectance spectrum of the substrate (CB) was compared to the corresponding spectrum of PETN/CB to obtain a difference spectrum: PETN/CB-CB. Examining the MIR laser transflectance spectrum of PETN/Al reveals that several of the vibrational markers of the aliphatic nitrate ester can be readily identified by simple comparison with the reference MIR laser spectrum. Thus, the only prerequisite for the application of this type of remote detection experiment is to acquire a MIR laser spectrum of a non-HE coated part of the substrate surface.

### 3.3 Conclusions

A MIR laser spectroscopic system allowed the detection of HEs on matte substrates at low substrate loadings on three types non-reflective substrates
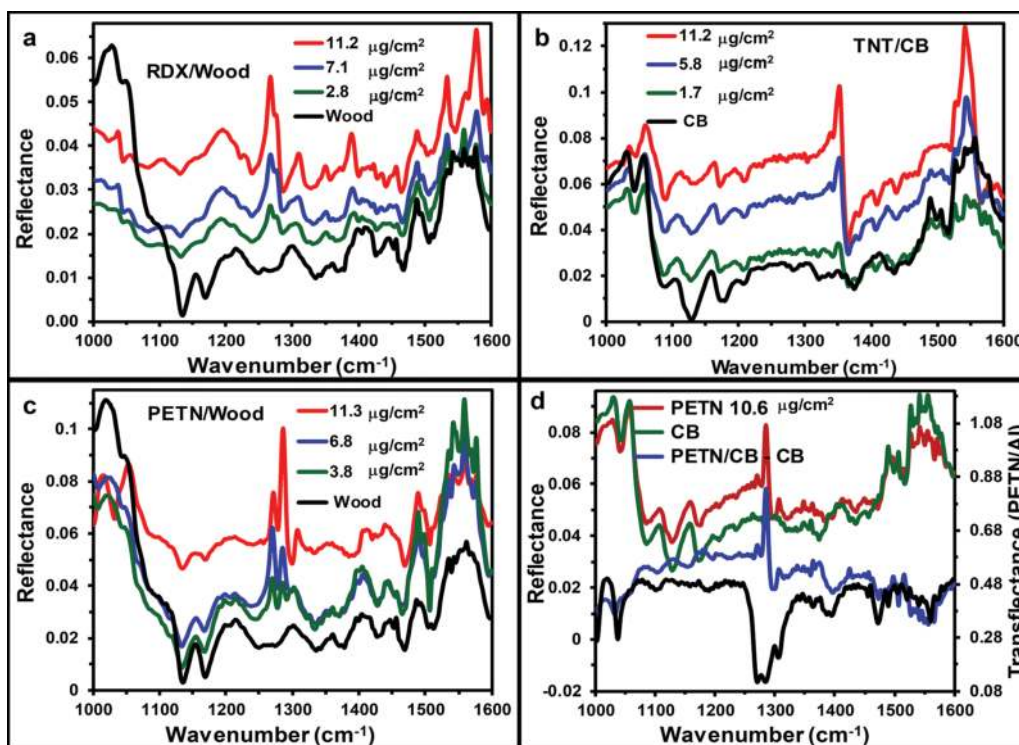


**Figure 4.**
*Surface concentration profiles for: (a) RDX/W; (b) TNT/CB; (c) PETN/W; (d) difference spectrum: PETN/CB-CB and QCL transflectance spectrum PETN/Al (Ref).*

investigated: TB, CB, and W. Spectral appearance of analytes deposited on substrates depend markedly on the optical properties of the substrate, namely the reflectivity of the surface. For metallic surfaces such as Al and SS, the reflectance spectra are similar to the transmission spectra of the analytes. For non-reflective substrates such as the ones used in this study, transflection spectra are observed that are similar to reflectance spectra with distorted band shapes, where $NO_2$ group bands dominate. Spectral identification using spectral correlation algorithms are generally insufficient for identifying the analytes when present as surface contaminants on strong MIR absorbing substrates. Nevertheless, MVA routines were adequately robust to attain the objectives of this research. The MVA routines used to identify the target HEs and to discriminate HEs from other HEs and the matte substrates serving as hosts for the explosives deposited on them required only the 1st dvt and MC as pretreatment algorithms for the spectroscopic data. Creating proficient PLS-DA models for W substrates was a much harder challenge, preprocessing a third step (SNV) to achieve the sought discrimination on W surfaces. Furthermore, classifications based on HEs were also achieved. A generalized PLS-DA model involving all HEs on all substrates permitted the discrimination even in the presence of strongly MIR absorbing and matte matrices, although the model relied on 12 LVs to capture a variance of 80%.

MIR laser spectroscopy was proven valuable for developing fast detection methods for detection of HEs on matte substrates. When HE is present on low reflectivity, high MIR absorbing surfaces coupling with MVA routines such as PLS and PLS-DA, identification and efficient discrimination of the HEs from the matte substrates was achieved. Moreover, when a reference spectrum of the matte surface can be obtained previous to obtaining the HE/surface reflectance spectrum, then the HE can be readily identified from a single spectroscopic measurement. Chemometrics routines can be used to create a more statistically sound methodology. PLS models were capable of predicting the surface loadings of explosives on substrates investigated using eight LVs or less to obtain regression coefficients squared values >0.9 [44, 57].

## 4. MIR laser spectroscopy assisted by classical least squares

Remote sensing using IRS depends on the range: observer-target distance. Other important factors to consider are the angle between source-target-detector and the reflectivity of the target. In the search for attaining higher return signals in back reflection mode, a QCL spectrometer was used to determine the presence of HE on cotton and other fabrics. The identification of vibrational signals was generated by a simple spectral comparison using classical least squares (CLS) in the minimization of the difference between real spectra (RS) and calculated spectra (CS). The models used for obtaining CS were based on linear combinations of HE spectra, cotton spectra, and biases. The QCL spectrometer was equipped with a 3″ diam. Convex ZnSe lens, which had three purposes: to focus the MIR light beam on the sample at 15 cm, to collect the reflected light, and to direct the light onto an internal MCT detector. Wavenumber precision and accuracy were 0.2 and 0.5 $cm^{-1}$, respectively. The optimum reflectance measurements were obtained at 15 ± 3 cm.

Experiments considering binary, ternary, and quaternary combinations of components such as cotton (and other fibers), TNT, RDX, and PETN were performed. The parameters calculated for the linear combination of the calculated spectrum were used to generate a discriminant analysis to determine the sensibility and specificity. Also, the extracted spectral signals of several amounts of RDX ($m_{RDX} \geq 0.02$ mg) deposited on the cotton substrates were used to calculate the

LOD value from the calculated S/Ns, which were determined from several spectra of cotton with different amounts of RDX in decreasing order until the S/N was ~3. Several DA schemes were successful in distinguishing the HE signals from those of the fabric substrates, but identification of HEs on cotton fabrics was achieved without the MVA used for discrimination.

The HEs samples were deposited on cotton and other fabrics by direct download of the solid. Two types of procedures were used for HE deposition. First, an amount of HE was deposited on glass, then the fabrics substrates were placed in contact with the HE/glass, and the HE was forced to be transferred using a thumbprint. In the second procedure, a metallic tip was pressed against a deposit of HE, and small quantities (particles) of the HE were transferred to the tip. Then these particles were deposited onto the fabrics. The fabrics were weighted before and after the transfer of the HEs to know the quantities deposited. Mass measurements were done using two scales. The first scale used for depositions of 3–0.1 mg, had a precision of ±0.1 mg. The second scale (thermogravimetric analysis scale) used for deposition of HE samples of masses ≤0.1 mg, had a precision of ±0.01 μg.

CLS can be considered as the transition between univariate and multivariate procedures of analysis. It is the most used regression method in academic environments since it is based on the Beer-Lambert–Bouguer linear relationship between the absorbance of a chemical species in a mixture of a solute and solvent, the path length of the light through the cell containing the mixture and the molar concentration of the species. Its familiarity among practitioners and students is based on the fact that for dilute solutions, it is directly applicable to quantitative spectral analyses [58].

CLS analysis can be easily extended to multi-component systems, where a wide range of peaks of several components in a mix is involved in the study. Typically, comprehensive information of the discrete constituents in the matrix studied is essential. This requirement is the greatest limitation of the regression analysis algorithm. Thus, the spectrum of each of the neat component as well as the spectrum of the mix is required to be able to estimate the spectral portion of each constituent in the mix. This is correct only when pure constituents are involved. The intensity at any wavenumber can be treated as a linear arrangement of the intensities of each constituent in the mix. The technique also estimates the portion of each spectrum constituent in the spectrum of the mix by minimizing the sum of the squares of the errors. Typically, this is equal to or linearly related to the percentage in the mix.

Two components, three components, and four components mixes were made from the four (4) constituents in the calibration set: three explosives: TNT, RDX, PETN, and the substrates: cotton, synthetic fabric or a mixed fabric. CLS analysis was coupled to QCL reflectance measurements of the four components and their mixes with the objective of developing a methodology for fast detection and discrimination analysis HE on fabrics. A simple technique for visualization of the data and interpretation of the models is presented. PLS-DA-based analysis requires the generation of independent models for each fabric type. This makes this MVA routine very hard to adapt to field detection of HEs. In the proposed CLS application, adapting the models to field work requires adding the spectra of new HEs or new substrates types to the database.

QCL diffuse reflectance spectra of all components and mixes were acquired using a rough gold substrate as background reference. Reflectance units (R) were converted to [−log(R)] to be used in the Chemometrics analysis of the data. **Figure 5** contains typical spectra obtained for the HEs and the fabrics. Normalization of the spectral data was achieved using SNV as preprocessing algorithm, applied to the whole spectroscopic range studied to remove the baseline drifts caused by scattering based on variations in particle size of the analytes (HEs) and the morphology of the substrates.
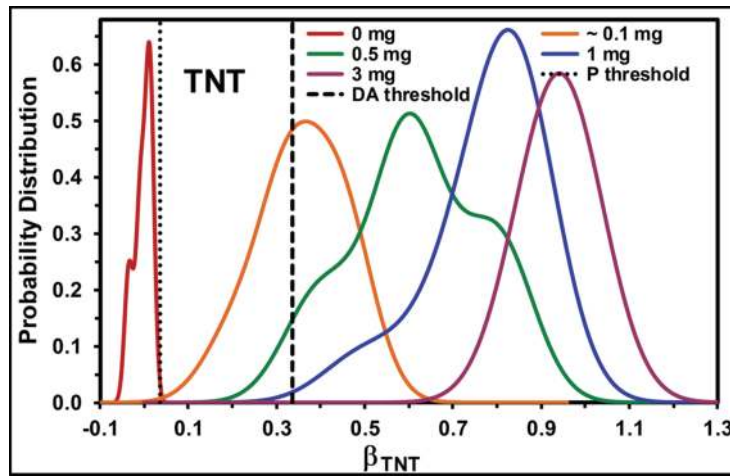
**Figure 5.**
*Kernel probability distribution of the $\hat{\beta}_{TNT}$ parameter for TNT/cotton binary mix.*

## 4.1 Statistical models

Spectra were acquired in SPC file format for spectroscopy (Thermo-Galactic Grams/AI™, Thermo-Fisher Scientific, Inc., Waltham, MA, USA) and analyzed using a CLS algorithm coded in Matlab™ (The MathWorks, Inc., Natick, MA, USA). PLS Toolbox v. 8.1 (Eigenvector Research, Inc., Manson, WA, USA) was used to generate the matrices for other MVA. Other statistical routines were implemented using Statgraphics Centurion XV software, version 15.2.05. (Statpoint Technologies, Inc. Warrenton, VA, USA). The linear model based on CLS can be described by [58].

$$f\left(\varphi_j, \hat{\beta}_j\right)_i = \hat{\beta}_0 + \hat{\beta}_1 \varphi_1(\omega_i) + \cdots + \hat{\beta}_j \varphi_j(\omega_i) \tag{1}$$

Here, $(\varphi_j, \hat{\beta}_j)_i$ $i$ represents the $i$th intensity, normalized, of the spectrum with intensities calculated in $[-\log(R)]$ units, from a mix of several constituents ($j$); $\varphi_j(\omega_i)$ is the intensity at each wavenumber ($\omega_i$) of the net spectrum belonging to the j component, and $\hat{\beta}_j$ is a parameter that indicates the portion of the spectrum of a given constituent in the spectrum of the mix. It has been assumed that there are no interactions among the components in the mix leading to chemical bonds. If present, these interactions would result in changes in intensities, shifts of band locations and formation or loss of vibrational bands due to the chemical bonds formed. Thus, at least to first order, the contributions to a given intensity are additive. The $\hat{\beta}_j$ were estimated by computing the minimum value of the square of the difference between the real (RS) and the calculated spectra (CS) according to:

$$d_i = y_i - \hat{f}\left(\varphi_j, \hat{\beta}_j\right)_i \tag{2}$$

The minimum of the sum of the squares of the residuals ($d_i$) with respect to $\hat{\beta}_j$ can be obtained by calculating the first-order partial derivatives with respect to $\hat{\beta}_j$, equating them to zero and calculating the values for $\hat{\beta}_j$. This leads to a set of "$n$" parameters, which represent "$n$" partial-derivative equations:

$$\frac{\partial d^2}{\partial \beta_j} = -2 \sum_i d_i \frac{\partial f\left(\hat{\varphi}_j, \hat{\beta}_j\right)_i}{\partial \hat{\beta}_j} = 0, \quad j = 1, 2, \cdots, n \tag{3}$$

The signals of interest for each constituent of the mix can be extracted from the model. For instance, for constituent 1, the extracted spectrum ($\hat{\psi}$) is

$$\hat{\psi}_{1(\omega_i)} = y_i - \hat{\beta}_0 - \hat{\beta}_2 \varphi_2(\omega_i) - \cdots - \hat{\beta}_j \varphi_j(\omega_i) \tag{4}$$

Three types of CLS models were created, according to the constituents in the mix: 2, 3, and 4-constituent models. One of the binary models consisted only in spectra of the fabric and one of the HEs. Thus, Eq. (1) now becomes:

$$f_{cotton}^{HE} = \hat{\beta}_0 + \hat{\beta}_{cotton} \varphi_{cotton}(\omega_i) + \hat{\beta}_{HE} \varphi_{HE}(\omega_i) \tag{5}$$

A total of 12 samples containing surface loadings of HEs in the range of 0.1–3 mg were prepared. The $\hat{\beta}_{HE}$ values were calculated from five replicate spectra acquired at various positions on the surface for the various sample concentrations, resulting in a total of 60 spectra. Probability distributions were then predicted. P-models for each of the HE/substrate binary combinations were generated. The p-values of the models were used as decision thresholds. These values were determined by using the projected average value ($\bar{x}$) of $\hat{\beta}_{HEM}$ for the cotton fabric substrates (controls) and standard deviations ($s_d$) according to:

$$p = \bar{x} + 3.28 \cdot s_d \tag{6}$$

From the definition of the LOD, the random error was estimated at 5% [42–44]. This implies that there is a high probability that non-dosed substrates were below the threshold. To obtain good discrimination typical spectra of the fabric substrates were required to be present in the database. As shown in **Table 2**, the models generated were characterized with high selectivity and sensitivity for the HEs in the range of 0.1–3 mg. The CLS-based model was compared with a discriminant analysis (DA) model. **Table 2** contains the results, where the value of $\hat{\beta}_{HE}$ was used to create a model for discrimination. The difference between the CLS model and the DA model is in the calibration. The CLS model required a spectrum of the substrate (cotton) without the presence of HEs (no HE) and with the reflectance spectra of the HEs (no substrate). There is no need to include HEs/substrates spectra. **Figure 5** shows the estimation of the probability for TNT in the range of 0.1–3 mg vs. $\hat{\beta}_{TNT}$.

The spectra for the two-component models for the HEs are shown in **Figure 6a–c**. In each of these graphs, the spectra with ~0.1 mg of the HE/cotton fabric substrates are shown in blue. Predicted spectra from Eq. (5) are in red. Reference spectra for the powder form of the HEs ("Ref") and cotton fabric substrates are in black and orange, respectively. The HE/cotton spectra with the cotton fabric spectra subtracted using Eq. (5) are in green. The two-components model that consists of cotton fabric and RDX spectra is shown as an example. The equation used was based on Eq. (5):

$$f_{cotton}^{RDX} = \hat{\beta}_0 + \hat{\beta}_{cotton} \varphi_{cotton}(\omega_i) + \hat{\beta}_{RDX} \varphi_{RDX}(\omega_i) \tag{7}$$

The equation for three-components models (cotton, TNT, RDX) following Eq. (1) is:

$$f_{cotton}^{TNT+RDX} = \hat{\beta}_0 + \hat{\beta}_{cotton} \varphi_{cotton}(\omega_i) + \hat{\beta}_{TNT} \varphi_{TNT}(\omega_i) + \hat{\beta}_{RDX} \varphi_{RDX}(\omega_i) \tag{8}$$

Three components mixes were composed of TNT, RDX, and fabric substrates. The sample set included 12 samples each in the range of 0.1–3 mg of 100% TNT and % RDX (24 samples) and 134 samples of binary mixtures of 50% TNT/RDX in the

| Component | CLS model | | Discriminant model | |
|---|---|---|---|---|
| | Sensitivity | Specificity | Sensitivity | Specificity |
| | **Binary** | | **Binary** | |
| Cotton | 100% | 100% | 100% | 89% |
| TNT | 100% | 100% | 89% | 100% |
| Cotton | 100% | 100% | 100% | 85% |
| RDX | 100% | 100% | 85% | 100% |
| Cotton | 100% | 100% | 100% | 95% |
| PETN | 100% | 100% | 95% | 100% |
| | **Ternary** | | **Ternary** | |
| Cotton | 100% | 100% | 100% | 86% |
| TNT | 100% | 97% | 94% | 100% |
| RDX | 99% | 88% | 91% | 100% |
| HEM | 100% | 100% | 86% | 100% |
| | **Quaternary** | | **Quaternary** | |
| Cotton | 100% | 100% | 100% | 88% |
| TNT | 89% | 94% | 86% | 90% |
| RDX | 95% | 84% | 86% | 100% |
| PETN | 99% | 67% | 86% | 91% |
| HEM | 100% | 100% | 88% | 100% |

**Table 2.**
*Sensitivity and specificity values for CLS and DA models.*

range of 0.5–3 mg deposited on cotton fabric. These were treated in the same way as for binary mixes. The values of $\hat{\beta}_{TNT}$ and $\hat{\beta}_{RDX}$ were estimated and the distribution plot for each sample from Eq. (8).

Quaternary mixes containing TNT, RDX, PETN, and fabrics can be described by:

$$f_{cotton}^{HEs} = \hat{\beta}_0 + \hat{\beta}_{cotton}\,\varphi_{cotton}(\omega_i) + \hat{\beta}_{TNT}\,\varphi_{TNT}(\omega_i) + \hat{\beta}_{RDX}\,\varphi_{RDX}(\omega_i) + \hat{\beta}_{PETN}\,\varphi_{PETN}(\omega_i) \quad (9)$$

Four components mixes were similar to three-component mixes with the addition of PETN. A total of 252 samples of 100% TNT, RDX, and PETN in the mass range of 0.1 to 3 mg and 50% mixes of TNT/RDX, TNT/PETN, PETN/RDX, and 33.3% mixes of TNT/PETN/RDX, each in the range of 0.5–3 mg were transferred onto cotton substrates. The values for $\hat{\beta}_{TNT}\hat{\beta}_{RDX}$, and $\hat{\beta}_{PETN}$ for the mixes were estimated together with their distribution plot for each sample from Eq. (9). **Table 2** contains the calculated values for the sensitivity and specificity. Comparison of reference spectra of HE and a spectrum for the quaternary mixture TNT-RDX-PETN/cotton is illustrated in **Figure 6d**.

A DA was done with the purpose of evaluating the discriminating capacity of the $\beta$ parameters. Discriminating functions (F1, F2, and F3) were obtained. The functions captured nearly all the statistically pertinent information of the DA, contributing to 95.3% of the discrimination. Eigenvalues for the discriminant functions were highly significant ($p < 0.0001$). **Table 3** shows the values for the canonical correlation coefficient, which is indicative of the efficiency for discriminating new samples, the functions showed excellent capabilities for determining group differences: 93% (F1), 87% (F2), and 77% (F3). F3 was not as effective as the other two
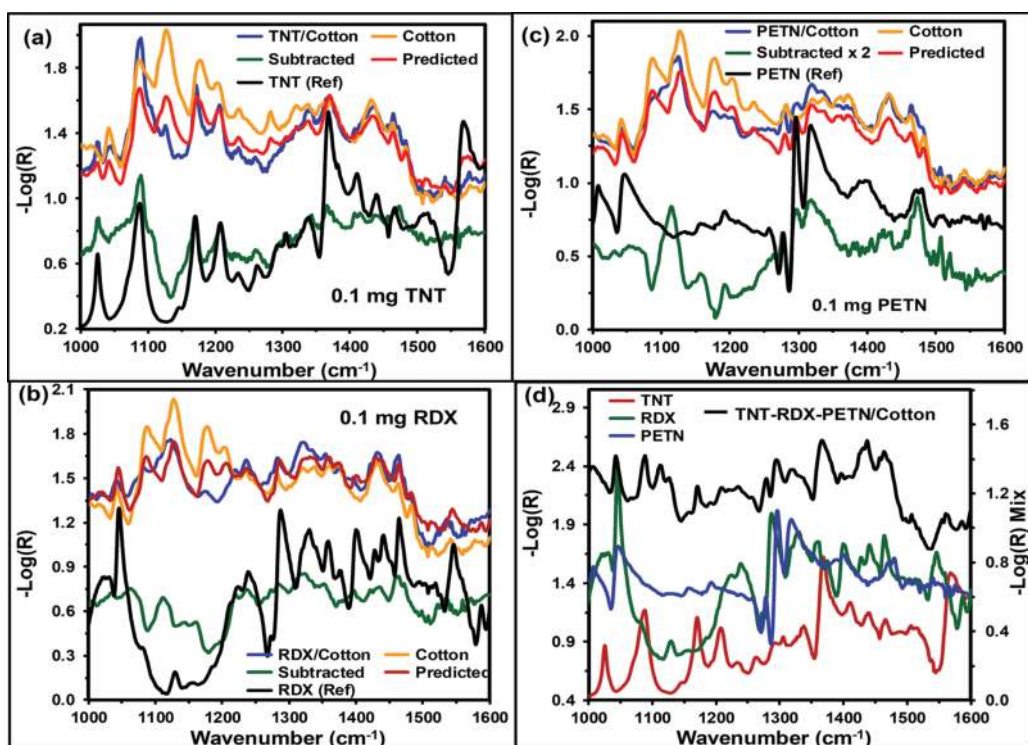
**Figure 6.**
*(a–c) Spectra of ~0.1 mg of HE/cotton (blue); predicted spectra from Eq. (5) (red traces); cotton spectra (orange); subtraction of the cotton spectra from HE/cotton spectra calculated using Eq. (4) (green); reference HE spectra (black); (d) comparison of reference spectra of HE and a spectrum for the quaternary mixture: TNT-RDX-PETN/cotton.*

| Discriminant analysis | | | |
|---|---|---|---|
| Discriminant function | 1 | 2 | 3 |
| Eigenvalue | 6.2 | 3.2 | 0.5 |
| Relative % | 63% | 32% | 5% |
| Canonical correlation | 0.93 | 0.87 | 0.56 |
| Wilks Lambda | 0.02 | 0.16 | 0.68 |
| Chi-squared | 901.9 | 431.7 | 90.6 |
| p value | <0.0001 | <0.0001 | <0.0001 |

**Table 3.**
*Values of statistical parameters of functions derived from the $\hat{\beta}_{HE}$ parameters.*

DA functions. The value for the LOD was calculated from various spectra of RDX at low surface loadings (<0.1 mg). The RDX vibrational signatures were in assigned and Eq. (4) was applied to the laser reflectance spectra. Then S/Ns were calculated for two signals (1040 and 1463 cm$^{-1}$). An S/N of 3 represented a mass of 22 ± 6 μg. According to the IUPAC definition, this is the LOD. Other methods for calculating the LOD lead to values ranging from 15 to 58 μg RDX.

## 4.2 Tests with other substrates

Other fabrics were tested as substrates (5 in total). These included 100%, cotton (white T-shirt), 100% polyester, 65% polyester/35% cotton, 45% polyester/55% cotton, and 84% polyester/16% Spandex™. Spectra for the clean substrates (no HEs)
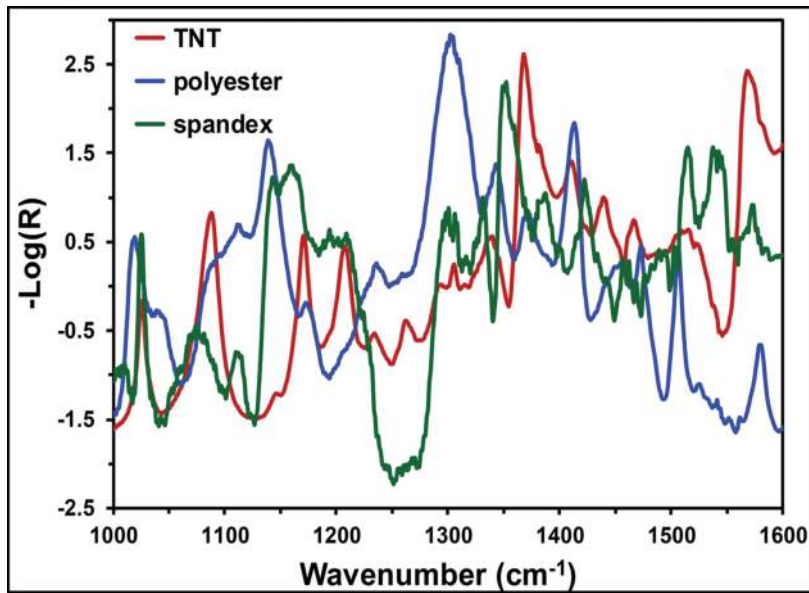
**Figure 7.**
*QCL reflectance spectra of components used in the additional tests of the proposed methodology based on CLS: TNT, polyester and Spandex™.*

and spectra of substrates dosed with TNT were acquired. **Figure 7** shows the MIR laser spectra of TNT, polyester, and Spandex™ used for the three additional models generated. First, a two-component model was generated with TNT as HE, based on Eq. (5). This model consisted of a spectrum for blue jeans cotton and a spectrum of TNT. **Table 4** contains the information resulting from the study. All substrates containing TNT were predicted correctly. Nevertheless, some of the samples containing polyester and Spandex™ (no TNT) were predicted as having TNT, i.e., as false positives. Except for the samples of white cotton substrates, $\hat{\beta}_{TNT}$ values were high, since the model previously incorporated a spectrum of cotton from blue jeans. High $\hat{\beta}_{TNT}$ values were predicted for samples with low amounts of TNT (~0.1 mg). This was unexpected since $\hat{\beta}_{TNT}$ values should have been low. In spectra of samples of polyester and spandex polymer substrates the result can be explained based on the fact that these substrates have intense peaks in the same spectral range as TNT.

Spectra of cotton, polyester, and TNT were used to build another model. Then the spectrum of polyester was included in the model resulting in samples with this substrate were correctly predicted with values of $\hat{\beta}_{TNT}$ close to zero. Samples of Spandex™ substrate were incorrectly classified. A third model was created by adding the spectrum of Spandex™ to the second model. This resulted in a correct classification of all samples. Moreover, samples with low amounts of TNT (~0.1 mg) had a low value of $\hat{\beta}_{TNT}$ (**Table 4**). This further confirms the hypothesis in order to have a good prediction ability for CLS models developed it is important to include the spectra of all components, including spectra of neat substrates. For practical identification of HEs on fabrics in defense and security applications, the database to be built must contain the spectrum of the target HE, as well as the spectra for the substrate and the other components in the matrix. Moreover, this important result leads to the conclusion that the model is forward adaptive, both to "new" HEs and "new" substrates.

## 4.3 Conclusions

Reconceptualization of CLS procedure in combination MIR laser spectroscopy resulted in a protocol for detection of HEs in mixes. The ability of the MIR laser

| Sample | Model 1 $(\hat{\beta}_{TNT})$ | Model 2 $(\hat{\beta}_{TNT})$ | Model 3 $(\hat{\beta}_{TNT})$ |
|---|---|---|---|
| White cotton | $-0.05 \pm 0.01$ | $-0.07 \pm 0.01$ | $-0.06 \pm 0.01$ |
| Polyester | **$0.15 \pm 0.05$** | $-0.01 \pm 0.03$ | $0.00 \pm 0.02$ |
| 65% polyester 35% cotton | **$0.15 \pm 0.03$** | $-0.05 \pm 0.03$ | $-0.01 \pm 0.03$ |
| 45% polyester 55% cotton | **$0.04 \pm 0.04$** | $-0.03 \pm 0.03$ | $-0.07 \pm 0.03$ |
| 84% polyester 16% spandex | **$0.31 \pm 0.03$** | **$0.17 \pm 0.03$** | $0 \pm 0.03$ |
| 2 mg TNT 65% polyester 35% cotton | $0.83 \pm 0.04$ | $0.78 \pm 0.04$ | $0.68 \pm 0.05$ |
| 0.5 mg TNT 65% polyester 35% cotton | $0.5 \pm 0.1$ | $0.4 \pm 0.1$ | $0.3 \pm 0.1$ |
| 2 mg TNT 45% polyester 55% cotton | $0.72 \pm 0.08$ | $0.67 \pm 0.09$ | $0.58 \pm 0.09$ |
| 0.5 mg TNT 45% polyester 55% cotton | $0.38 \pm 0.02$ | $0.31 \pm 0.02$ | $0.27 \pm 0.03$ |
| 4 mg TNT on 84% polyester 16% spandex | $0.9 \pm 0.1$ | $0.9 \pm 0.1$ | $0.9 \pm 0.1$ |
| 2 mg TNT on 84% polyester 16% spandex | $0.3 \pm 0.1$ | $0.3 \pm 0.2$ | $0.5 \pm 0.2$ |
| 0.8 mg TNT on 84% polyester 16% spandex | $0.3 \pm 0.2$ | $0.2 \pm 0.2$ | $0.3 \pm 0.2$ |
| 0.5 mg TNT on 84% polyester 16% spandex | $0.4 \pm 0.1$ | $0.3 \pm 0.1$ | $0.2 \pm 0.2$ |
| ~0.1 mg TNT on 84% polyester 16% spandex | $0.25 \pm 0.01$ | $0.12 \pm 0.01$ | $0.05 \pm 0.01$ |

**Table 4.**
*Prediction of $\hat{\beta}_{TNT}$ parameters for the three models developed for additional fabrics.*

spectroscopy assisted by CLS for detection of 1, 2, and 3 HEs in solid mixes deposited on non-reflective surfaces, such as cotton, polyester and spandex fabrics, was demonstrated. Moreover, the adaptive learning ability of the models based on CLS was also demonstrated by performing discrimination with the spectra corresponding to the different substrate where the HE detection would occur. This important feature of the CLS models was demonstrated by adding spectra of five other substrates (fabrics) to the database. Neat substrates (no analyte present) and substrates containing TNT were investigated. For models that did not contain the spectra of the fabric substrate, false positives were obtained resulting in detection failure for samples with HEs. Thus, for the methodology to work, the model must be fed with the spectra for the fabric substrates and HEs.

RDX signals ($m_{RDX} > 0.02$ mg) on cotton fabrics were used to calculate the LOD. Values of S/N calculated from the spectra of cotton fabrics dosed with decreasing masses of RDX until S/N $\approx 3$ resulted in a LOD of 15–33 µg, depending on the spectroscopic signal used. Comparisons of dosed RDX mass with the fraction predicted led to linear fits which were also used to calculate LOD values based on the uncertainty of the blank and the slope of the fit. The LOD value resulting from this procedure was of 58 µg. Another way of calculating the LOD used an interpolation of the p-value threshold for low RDX dosage resulted in a value of 40 µg. This is probably the most representative value of the method LOD [59].

The minimum limit of quantification (LOQ) of surface concentrations was based on experiments performed on three-components mixes of RDX/PETN/cotton. The LOQ value for RDX was 10%. Vibrational markers for PETN and RDX could be readily observed for all samples except at 5% RDX (lowest concentration). Successful detection of RDX on cotton in the 10% RDX/90% PETN mix on cotton was achieved using the presented procedure.

Coupling of CLS to QCL reflectance data of analyte residues on fabrics enable a fast and efficient discrimination procedure providing an improved understanding and visualization of analyte/substrate reflectance signals. Since there is a nonlinear

dependence between the spectrum of the mix and the spectra of the neat components, quantification of HE/fabric is not easily achieved. However, this situation does not affect HEs detection on fabrics for all the cases studied. Further studies are required to determine if QCL-CLS detection of HE can be done on other matte substrates, particularly in the presence of interferents and other contaminants [57, 60].

## 5. Summary

MIR laser spectroscopy is a powerful spectroscopic analysis technique that has recently achieved significant acceptance in many fields of science and technology. When the reflectance spectra excited by a QCL system is coupled to the powerful MVA routines of Chemometrics, the results obtained are even further reaching, regarding the discriminating power, the LOD and LOQ, and the clustering of similar data and separation of dissimilar data of not easily correlated spectroscopic information. A selection of several applications of MIR laser spectroscopy has been presented that concentrating on the detection of HEs. The near and far future of the technique is as bright as the MIR lasers that shine on samples to enable design and development of new applications as well as revisiting other well established spectroscopic tools under highly enhanced conditions.

## Acknowledgements

## Author details

Leonardo C. Pacheco-Londoño[1,2], John R. Castro-Suarez[1,3], Nataly J. Galán-Freyle[1,2], Amanda M. Figueroa-Navedo[1], José L. Ruiz-Caballero[1], Ricardo Infante-Castillo[1,4] and Samuel P. Hernández-Rivera[1*]

1 Department of Chemistry, ALERT DHS Center of Excellence, University of Puerto Rico-Mayagüez, Mayagüez, PR, USA

2 School of Basic and Biomedical Sciences, Universidad Simón Bolívar, Barranquilla, Colombia

3 Antonio de Arévalo Technological Foundation, TECNAR, Cartagena, Colombia

4 Department of Physics-Chemistry, University of Puerto Rico, Arecibo, PR, USA

*Address all correspondence to: samuel.hernandez3@upr.edu

IntechOpen

## References

[1] Schraeder B. Early history of vibrational spectroscopy. In: Schrader B, editor. Infrared and Raman Spectroscopy: Methods and Applications. Weinheim, Germany (New York, NY): VCH; 1995. ISBN: 3-527-26446-9

[2] Sheppard N. The historical development of experimental techniques in vibrational spectroscopy. In: Chalmers JM, Griffiths PR, editors. Handbook of Vibrational Spectroscopy. Vol. 1. West Sussex England: Wiley, Chichester; 2002. 1 p. ISBN: 978-0-471-98847-2

[3] Griffiths PR. Introduction to vibrational spectroscopy. In: Chalmers JM, Griffiths PR, editors. Handbook of Vibrational Spectroscopy. Vol. 1. Chichester, West Sussex, England: Wiley; 2002. 33 p. ISBN: 978-0-471-98847-2

[4] Griffiths PR, de Haseth JA. Fourier Transform Infrared Spectrometry. 2nd ed. Hoboken, NJ: John Wiley & Sons, Inc.; 2007. ISBN: 978-0-471-19404-0

[5] Larkin P. Infrared and Raman Spectroscopy: Principles and Spectral Interpretation. 2nd ed. Waltham, MA, USA: Elsevier; 2018. ISBN: 978-0-12-804162-8

[6] Yinon J, Zitrin S. Modern Methods and Applications in Analysis of Explosives. Chichester, UK: John Wiley & Sons Ltd; 1996. ISBN: 978-0-471-96562-6

[7] Castro-Suarez JR, Ortiz-Rivera W, Galán-Freyle N, Figueroa-Navedo A, Pacheco-Londoño LC, Hernández-Rivera SP. Multivariate Analysis in Vibrational Spectroscopy of Highly Energetic Materials and Chemical Warfare Agents Simulants. DOI: 10.5772/54104

[8] Valim de Freitas L, Barbosa Rodrigues de Freitas AP. Multivariate Analysis in Management, Engineering and the Sciences. Rijeka, Croatia: InTech; 2013. DOI: 10.5772/3301. ISBN: 978-953-51-0921-1

[9] Steinfeld JI, Wormhoudt J. Explosives detection: A challenge for physical chemistry. Annual Review of Physical Chemistry. 1998;**49**:203-232. DOI: 0066-426X/98/1001-0203

[10] Committee on the Review of Existing and Potential Standoff Explosives Detection Techniques, Existing and Potential Standoff Explosives Detection Techniques. Washington, DC: National Research Council, National Academy of Sciences Committee; 2004. DOI: 10.17226/10998

[11] Parmenter JE. The challenge of standoff explosives detection. In: Proceedings of the 38th Annual International Carnahan Conference on Security Technology. New York, NY: IEEE; 2004. pp. 355-358

[12] Schubert H, Rimski-Korsakov A. Stand-off detection of suicide-bombers and mobile subjects. In: Proceedings of the NATO Advanced Research Workshop on Stand-off Detection of Suicide Bombers and Mobile Subjects, NATO Security through Science Series B: Physics and Biophysics, Pfinztal, Germany. Germany: Springer; 2005

[13] Moore DS. Instrumentation for trace detection of high explosives. The Review of Scientific Instruments. 2004;**75**:2499-2512. DOI: 10.1063/1.1771493

[14] Moore DS. Recent advances in trace explosives detection instrumentation. Sensing and Imaging. 2009;**8**(1):9-38. DOI: 10.1007/s11220-007-0029-8

[15] Marshall M, Oxley JC. Aspects of Explosives Detection. Amsterdam, The Netherlands: Elsevier; 2009. ISBN: 978-0-12-374533-0

[16] Caygill JS, Davis F, Higson SPJ. Current trends in explosive. Talanta. 2012;**88**:14-29. DOI: 10.1016/j.talanta.2011.11.043

[17] Tourné M. Developments in explosives characterization and detection. Journal of Forensic Research. 2013;**S12**:1-10. DOI: 10.4172/2157-7145.S12-002

[18] Fountain AW III, Christesen SD, Moon RP, Guicheteau JA. Recent advances and remaining challenges for the spectroscopic detection of explosive threats. Applied Spectroscopy. 2014;**68**(8):795. DOI: 10.1366/14-07560

[19] Carter JC, Angel SM, Lawrence-Snyder M, Scaffidi J, Whipple RE, Reynolds JG. Standoff detection of high explosive materials at 50 meters in ambient light conditions using a small Raman instrument. Applied Spectroscopy. 2005;**59**(6):769-775. DOI: 10.1366/0003702054280612

[20] Ortiz-Rivera W, Pacheco-Londoño LC, Castro-Suarez JR, Félix-Rivera H, Hernandez-Rivera SP. Vibrational spectroscopy standoff detection of threat chemicals. Proceedings of SPIE. 2011;**8031**(803129):803129-803110. DOI: 10.1117/12.884433

[21] Moros J, Lorenzo JA, Novotný K, Laserna JJ. Fundamentals of stand-off Raman scattering spectroscopy for explosive fingerprinting. Journal of Raman Specroscopy. 2013;**44**(1):121-130. DOI: 10.1002/jrs.4138

[22] Wallin S, Pettersson A, Östmark H, Hobro A. Laser-based standoff detection of explosives: A critical review. Analytical and Bioanalytical Chemistry. 2009;**395**(2):259-274. DOI: 10.1007/s00216-009-2844-3

[23] Galán-Freyle NJ, Pacheco-Londoño LC, Figueroa-Navedo AM, Hernandez-Rivera SP. Standoff detection of highly energetic materials using laser-induced thermal excitation of infrared emission. Applied Spectroscopy. 2015;**69**(5):535-544. DOI: 10.1366/14-07501

[24] Castro-Suarez JR, Pacheco-Londoño LC, Vélez-Reyes M, Diem M, Tague TJ, Hernandez-Rivera SP. FT-IR standoff detection of thermally excited emissions of trinitrotoluene (TNT) deposited on aluminum substrates. Applied Spectroscopy. 2013;**67**(2):181-186. DOI: 10.1366/11-06229

[25] Pacheco-Londoño LC, Ortiz-Rivera W, Primera-Pedrozo OM, Hernández-Rivera SP. Vibrational spectroscopy standoff detection of explosives. Analytical and Bioanalytical Chemistry. 2009;**395**(2):323-335. DOI: 10.1007/s00216-009-2954-y

[26] Pettersson A, Johansson I, Wallin S, Nordberg M, Östmark H. Near real-time standoff detection of explosives in a realistic outdoor environment at 55 m distance. Propellants, Explosives, Pyrotechnics. 2009;**34**(4):297-306. DOI: 10.1002/prep.200800055

[27] Faist J, Capasso F, Sivco DL, Sirtori C, Hutchinson A, Cho AY. Quantum cascade laser. Science. 1994;**264**(5158):553-556. DOI: 10.1126/science.264.5158.553

[28] Faist J, Capasso F, Sirtori C, Sivco DL, Baillargeon JN, Hutchinson AL, et al. High power mid-infrared ($\lambda \sim 5$ μm) quantum cascade lasers operating above room temperature. Applied Physics Letters. 1996;**68**(26):3680-3682. DOI: 10.1063/1.115741

[29] Capasso F, Gmachl C, Paiella R, Tredicucci A, Hutchinson AL, Sivco DL, et al. New frontiers in quantum cascade lasers and applications. IEEE Journal of Selected Topics in Quantum Electronics. 2000;**6**:931. DOI: 10.1109/2944.902142

[30] Gmachl C, Capasso F, Sivco DL, Cho AY. Recent progress in quantum cascade lasers and applications. Reports on Progress in Physics. 2001;**64**:1533. DOI: 10.1088/0034-4885/64/11/204

[31] Beck M, Hofstetter D, Aellen T, Faist J, Oesterle U, Ilegems M, et al. Continuous wave operation of a mid-infrared semiconductor laser at room temperature. Science. 2002;**295**(5553):301-305. DOI: 10.1126/science.1066408

[32] Mizaikoff B, Lendl B. Sensor systems based on mid-infrared transparent fibers. In: Chalmers JM, Griffiths PR, editors. Handbook of Vibrational Spectroscopy. Vol. 2. Chichester, West Sussex, England: Wiley; 2002. ISBN: 978-0-471-98847-2

[33] Razeghi M. High-performance InP-based mid-IR quantum cascade lasers. IEEE Journal of Selected Topics in Quantum Electronics. 2009;**15**:941. DOI: 10.1109/JSTQE.2008.2006764

[34] Razeghi M. High-power high-wall plug efficiency mid-infrared quantum cascade lasers based on InP/GaInAs/InAlAs material system. Proceedings of SPIE. 2009;**7230**:723011. DOI: 10.1117/12.813923

[35] Pushkarsky MB, Dunayevskiy IG, Prasanna M, Tsekoun AG, Go R, Patel CKN. High sensitivity detection of TNT. Proceedings of the National Academy of Sciences of the United States of America. 2006;**103**(52):19630-19634. DOI: 10.1073/pnas.0609789104

[36] Patel CKN. Laser based In-situ and standoff detection of chemical warfare agents and explosives. Proceedings of SPIE. 2009;**7484**:748402-1-78401-14. DOI: 10.1117/12.835883

[37] Bauer C, Willer U, Schade W. Use of quantum cascade lasers for detection of explosives: Progress and challenges. Optical Engineering.

2010;**49**(11):111126-111126-7. DOI: 10.1117/1.3498771

[38] Pacheco-Londoño LC, Castro-Suarez JR, Hernández-Rivera SP. Detection of nitroaromatic and peroxide explosives in air using infrared spectroscopy: QCL and FTIR. Advanced Optical Technologies. 2013;**2013**:8 p. Article ID: 532670. DOI: 10.1155/2013/532670

[39] Van Neste CW, Senesac LR, Thundat T. Standoff spectroscopy of surface adsorbed chemicals. Analytical Chemistry. 2009;**81**:1952-1956. DOI: 10.1021/ac802364e

[40] Hildebrand J, Herbst J, Wöllenstein J, Lambrecht A. Explosive detection using infrared laser spectroscopy. Proceedings of SPIE. 2009;**7222**:72220B. DOI: 10.1117/12.808976

[41] Fuchs F, Hugger S, Kinzer M, Aidam R, Bronner W, Losch R, et al. Imaging standoff detection of explosives using widely tunable mid infrared quantum cascade lasers. Optical Engineering. 2010;**49**(11):111127-111127-8. DOI: 10.1117/1.3506195

[42] Deutsch ER, Kotidis P, Zhu N, Goyal AK, Ye J, Mazurenko A, et al. Active and passive infrared spectroscopy for the detection of environmental threats. Proceedings of SPIE. 2014;**9106**:91060A-9. DOI: 10.1117/12.2058544

[43] Suter JD, Bernacki B, Phillips MC. Spectral and angular dependence of mid-infrared diffuse scattering from explosives residues for standoff detection using external cavity quantum cascade lasers. Applied Physics B: Lasers and Optics. 2012;**108**(4):965-974. DOI: 10.1007/s00340-012-5134-2

[44] Castro-Suarez JR, Pollock YS, Hernández-Rivera SP. Explosives detection using quantum cascade

laser spectroscopy. Proceedings of SPIE. 2013;**8710**:871010. DOI: 10.1117/12.2016037

[45] Pacheco-Londoño LC, Castro-Suarez JR, Aparicio-Bolaños J, Hernández-Rivera SP. Angular dependence of source-target-detector in active mode standoff infrared detection. Proceedings of SPIE. 2013;**8711**:8711081-8711086. DOI: 10.1117/12.2016153

[46] Ortega-Zúñiga CA, Galán-Freyle NY, Castro-Suarez JR, Aparicio-Bolaños J, Pacheco-Londoño LC, Hernández-Rivera SP. Dependence of detection limits on angular alignment, substrate type and surface concentration in active mode standoff IR. Proceedings of SPIE. 2013;**8734**:87340R-1-87340R-8. DOI: 10.1117/12.2016196

[47] Castro-Suarez JR, Pacheco-Londoño LC, Aparicio-Bolaño J, Hernandez-Rivera SP. Active mode remote infrared spectroscopy detection of TNT and PETN on aluminum substrates. Journal of Spectroscopy. 2017;**2017**:2730371

[48] Figueroa-Navedo AM, Galán-Freyle NJ, Pacheco-Londoño LC, SP H-R. Chemometrics enhanced laser induced thermal emission detection of PETN and RDX. Journal of Chemometrics. 2015;**29**:329-337

[49] Barker M, Rayens W. Partial least squares for discrimination. Journal of Chemometrics. 2003;**17**(3):166-173. DOI: 10.1002/cem.785

[50] Brereton RG. Chemometrics for Pattern Recognition. Chichester, England. The Atrium, Southern Gate: John Wiley & Sons Ltd.; 2009. ISBN: 978-0-470-98725-4

[51] Ballabio D, Consonni V. Classification tools in chemistry. Part 1: linear models. PLS-DA. Analytical Methods. 2013;**5**(16):3790-3798. DOI: 10.1039/C3AY40582F

[52] Clarkson J Smith WE, Batchelder DN, Smith DA, Coats AM. A theoretical study of the structure and vibrations of 2,4,6-trinitrotoluene. Journal of Molecular Structure. 2003;**648**(3):203-214. DOI: 10.1016/S0022-2860(0e3)00024-3

[53] Perger WF, Zhao J, Winey JM, Gupta YM. First-principles study of pentaerythritol tetranitrate single crystals under high pressure: Vibrational properties. Chemical Physics Letters. 2006;**428**(4):394-399. DOI: 10.1016/j.cplett.2006.07.046

[54] Prasad RL, Prasad R, Bhar GC, Thakur SN. Photoacoustic spectra and modes of vibration of TNT and RDX at $CO_2$ laser wavelengths. Spectrochimica Acta, Part A: Molecular and Biomolecular Spectroscopy. 2002;**58**(14):3093-3102. DOI: 10.1016/S1386-1425(02)00071-9

[55] Karpowicz RJ, Brill TB. Comparison of the molecular structure of hexahydro-I, 3,5-trinitro-s-triazine in the vapor, solution, and solid phases. The Journal of Physical Chemistry. 1984;**88**(3):348-352. DOI: 10.1021/j150647a005

[56] Infante-Castillo R, Pacheco-Londoño L, Hernández-Rivera SP. Vibrational spectra and structure of RDX and its $^{13}$C- and $^{15}$N-labeled derivatives: A theoretical and experimental study. Spectrochimica Acta A. 2010;**76**(2):137-141. DOI: 10.1016/j.saa.2010.02.051

[57] Castro-Suarez JR, Hidalgo-Santiago M, Hernández-Rivera SP. Detection of highly energetic materials on non-reflective substrates using quantum cascade laser spectroscopy. Applied Spectroscopy. 2015;**69**(9):1023-1035. DOI: 10.1366/14-07626

[58] Gallagher NB, Blake TA, Gassman PL, Shaver JM, Windig W. Multivariate curve resolution applied

to infrared reflection measurements of soil contaminated with an organophosphorus analyte. Applied Spectroscopy. 2006;**60**(7):713-722. DOI: 0003-7028/06/6007-0713$2.00/0

[59] Long GL, Winefordner JD. Limit of detection: A closer look at the IUPAC definition. Analytical Chemistry. 1983;**55**(07):712A-724A. DOI: 10.1021/ac00258a724

[60] Pacheco-Londoño LC, Aparicio-Bolaño J, Galán-Freyle NJ, Román-Ospino AD, Ruiz-Caballero JL, Hernández-Rivera SP. Classical least squares-assisted mid-infrared (MIR) laser spectroscopy detection of high explosives on fabrics. Journal of Applied Spectroscopy. 2018 (The online version). DOI: 10.1177/0003702818780414